RESEARCH ARTICLE | JUNE 27 2024

Kinetic isotope effects on hydrogen/deuterium disordering and ordering in ice crystals: A Raman and dielectric study of ice VI, XV, and XIX ⊕

Alexander V. Thoeny ; Tobias M. Gasser ; Lars Hoffmann ; Markus Keppler; Roland Böhmer ;
Thomas Loerting ✉

Check for updates

View Online   Export Citation

Kinetic isotope effects on hydrogen/deuterium disordering and ordering in ice crystals: A Raman and dielectric study of ice VI, XV, and XIX
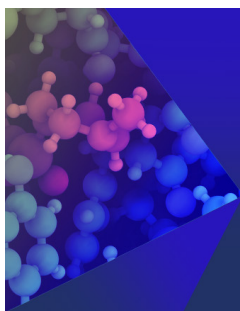
Alexander V. Thoeny,[1] (iD) Tobias M. Gasser,[1] (iD) Lars Hoffmann,[2] (iD) Markus Keppler,[2] Roland Böhmer,[2] (iD) and Thomas Loerting[1,a)] (iD)

AFFILIATIONS

[1] Institute of Physical Chemistry, University of Innsbruck, 6020 Innsbruck, Austria
[2] Fakultät Physik, Technische Universität Dortmund, 44221 Dortmund, Germany

Note: This paper is part of the JCP Special Topic on Water: Molecular Origins of its Anomalies.
[a)] Author to whom correspondence should be addressed: thomas.loerting@uibk.ac.at

ABSTRACT

Ice XIX and ice XV are both partly hydrogen-ordered counterparts to disordered ice VI. The ice XIX → XV transition represents the only order-to-order transition in ice physics. Using Raman and dielectric spectroscopies, we investigate the ambient-pressure kinetics of the two individual steps in this transition in real time (of hours), that is, ice XIX → transient ice VI (the latter called VI‡) and ice VI‡ → ice XV. Hydrogen-disordered ice VI‡ appears intermittent between 101 and 120 K, as inferred from the appearance and subsequent disappearance of the ice VI Raman marker bands. A comparison of the rate constants for the H_2O ices reported here with those from D_2O samples [Thoeny *et al.*, J. Chem. Phys. **156**, 154507 (2022)] reveals a large kinetic isotope effect for the ice XIX decay, but a much smaller one for the ice XV buildup. An enhancement of the classical overbarrier rate through quantum tunneling for the former can provide a possible explanation for this finding. The activation barriers for both transitions are in the 18–24 kJ/mol range, which corresponds to the energy required to break a single hydrogen bond. These barriers do not show an H/D isotope effect and are the same, no matter whether they are derived from Raman scattering or from dielectric spectroscopy. These findings favor the notion that a dipolar reorientation, involving the breakage of a hydrogen bond, is the rate determining step at the order-to-order transition.

I. INTRODUCTION

One of the many anomalies of water is its huge variety of crystal structures, comprising at least 20 ice polymorphs. A recent discovery is that of ice XIX, in 2021 independently reported by Yamane *et al.* and by some of us.[1,2] First evidence for the existence of ice XIX was presented in 2018 by combining results from x-ray diffraction, calorimetry, Raman scattering, and dielectric spectroscopy.[3] Ice XIX represents a hydrogen-ordered phase that exists at pressures of about 1–2 GPa. Its sibling phase, ice XV, can be described in the same manner. Yet, ice XIX is to be distinguished from ice XV in terms of the type of hydrogen order. Ice XIX preparation involves a synthesis protocol similar to that for ice XV. Both preparations start from ice VI but involve different pressures and cooling rates.[3]

At synthesis pressures below 0.85 GPa, mainly ice XV forms, while above 1.6 GPa, predominantly ice XIX forms.[4] Ices XV and XIX share the oxygen atom topology with ice VI, but they differ with respect to the arrangement of the H atoms: Ices XV and XIX are partly H ordered,[1,2,5] but ice VI is disordered. In other words, they are examples for H-lattice polymorphism. Pairs sharing the same oxygen lattice are common in ice physics,[5–9] while the triple of ice VI/XV/XIX is unique. Here, it has to be noted that ices VII, VIII, and X also share the same oxygen lattice.[10] Yet, in the ultrahigh pressure regime of ice X, water loses its molecular nature and turns into an atomic crystal.[10]

Ices XV and XIX both form from ice VI below 110–130 K. In that range, the thermal H-atom motion is slow and ordered phases start to be favored by entropy. The process of ordering,

however, does not happen unconditionally. Pure, disordered H_2O or D_2O ice phases typically undergo an orientational glass transition[9] at low temperatures, which immobilizes the H-atom network. In this situation, the missing molecular mobility prevents H/D ordering, even though thermodynamics would require it. In order to increase the mobility on the H/D atom sublattice, point defects are necessary. Commonly, these are combinations of ionic and Bjerrum defects that are introduced through doping.[6,9] For high-pressure ice modifications, HCl is usually the most suitable dopant.[11,12]

Typically, the rule is that the addition of these dopants is sufficient for H-ordering to occur on common laboratory time scales of hours. This statement holds even when the temperature for H-ordering is below the orientational glass transition temperature as, e.g., given for the H-order transition from ice VI to ice XV compared to the orientational glass transition of ice VI.[13] The one exception to this rule is deuterated ice XIX, for which the use of external ionic and Bjerrum defects is insufficient. That is, replacing D for H and following the protocol that successfully generates protiated ice XIX do *not* lead to deuterated ice XIX. An additional measure that we call "isotope doping" is required to enhance the dynamics further. Isotope doping involves the addition of minute amounts of H_2O to the D_2O/DCl parent solution. The H defects turn out to act as catalysts, crucially speeding up the formation of D_2O ice XIX.[1] Initially, the unresolved issue how to make deuterated ice XIX was the major obstacle on the way to determine the crystal structure of ice XIX using neutron powder diffraction. Moreover, the isotope doping issue has resulted in a misconception regarding the structure of ice XIX. Salzmann *et al.* report a crystal structure for a D-disordered phase made from pure D_2O/DCl and call it "ice XIX."[14] However, they did not employ the catalyst that was found necessary to actually produce deuterated ice XIX.[1] In his perspective, Komatsu[15] discussed apparent differences of ice XIX as compared to the phase reported by Salzmann *et al.*[14] Specifically, the lattice parameters evaluated by Salzmann *et al.* are smaller than those in ices VI, XV, and XIX.[1,2,5,14–16] Moreover, dielectric relaxation measurements reported by Yamane *et al.*[2] and some of us[3] cannot be explained through changes in distortions between ices VI and "XIX" according to Komatsu.[15]

Despite being synthesized near 2 GPa, ice XIX is kinetically stable at ambient pressure in liquid nitrogen.[1–3] Upon heating at ambient pressure, the transition sequence ice XIX → XV → VI is incurred.[1,3,4,17,18] That is, the transition sequence at ambient pressure represents the only known order–order–disorder transformation in ice physics.[1,3,4,17,18] It is, therefore, especially interesting to investigate this type of transition in detail.

In fact, the initial order-to-order part of this transition sequence does *not* involve a "direct" conversion from ice XIX to ice XV. Instead, ice XIX first evolves into a transition state that is H disordered in nature, from which ordered ice XV eventually emerges. We use the term ice VI‡ for that transition state and call it "transient ice VI."[1,4,17,18] This transition state has been identified through calorimetry, Raman spectroscopy, and neutron diffraction.[1,4,17,18] Accordingly, the ice XIX to XV transition can be decomposed into an ice XIX decay and an ice XV buildup at ambient pressure. Both of these processes take place simultaneously. In other words, the initially formed ice VI‡ reorders to produce ice XV. At the same time, however, more ice VI‡ is delivered from the

continued decay of ice XIX. The mere observation of ice VI‡ demonstrates that the ice XIX → VI‡ transition proceeds much faster than the ice VI‡ → XV transformation.[18]

Raman spectroscopy turns out to be suitable to quantify the ice XIX → VI‡ and the ice VI‡ → XV transitions in mutually independent ways.[18] Characteristic Raman marker bands for all three ice forms have been identified.[18] In particular, for the ice XIX decay, the decoupled OD/OH stretching bands can be utilized. The formation of ice XV can be traced through an intensity increase of the librational bands at 340/450 cm^{-1} relative to those typical for ice XIX at 390/410 cm^{-1}. Slightly less pronounced, also ice VI shows a distinct marker band in the librational range at 405/530 cm^{-1}. Based on the superposition of all these reference Raman bands, we previously studied the kinetics of these two processes for *deuterated* (H-doped) samples. Using an adapted Johnson–Mehl–Avrami–Kolmogorov (JMAK) model,[19] this allowed us to extract the corresponding rate constants k, Avrami exponents n, and activation energies E_A.[18]

In the present work, *protiated* samples (containing small fractions of D_2O) are investigated, thereby enabling the detection of decoupled OD-stretching vibrations. Thus, we will again use Raman superposition to quantify the fractions of the corresponding ices and then use these fractions to extract kinetic parameters from JMAK fits. Just like in Ref. 18, the rate constants k_H describing the ice XIX decay and the ice XV buildup of the protiated samples are obtained from isothermal waiting experiments. Combining the rates k_H from the H_2O doped samples with the rates k_D from the D_2O samples, this allows us to quantify the H/D kinetic isotopic effect (KIE),

$$\text{KIE} = \frac{k_H}{k_D}. \tag{1}$$

This quantity might be helpful to elucidate the mechanism underlying both steps of the ice XIX → XV transition. Isotopic substitution leads to a stronger differentiation of the different isotopologues, e.g., when larger distances affect H/D-hopping or when rigid lattices affect rotations of the whole H_2O/D_2O-molecule. In this context, the impact of quantum tunneling might also change. If the latter is operative, one typically observes rather large KIEs (between one and many orders of magnitude[20]) as compared to classical overbarrier H jumps or molecular reorientations.[21] Quantum tunneling is usually most significant when the particles are light and when the height and width of the potential barrier are reduced as in systems containing small intermolecular distances. Such a reduction can stem from sample contractions occurring at low temperatures and/or high densities. Examples include the ice I → XI transition[22] as well as the pressure-induced ice VIII → VII transition[23] and possibly the ice XII → XIV[24] transition at 100 K, where quantum tunneling was found to be relevant. Owing to the high density of ice XIX (1.33 g cm^{-3} at 1 bar) and relatively low transition temperature (near 100 K), it seems plausible that quantum tunneling could play a role also for the ice XIX → XV transition. In other words, the relatively high density of ice XIX combined with the low transition temperature might reduce the height and width of the barrier sufficiently to enable such effects.

For the deuterated samples, not only the rate constants but also the activation barriers for the ice XIX decay and the ice XV buildup have been evaluated.[18] The barrier relating to the ice XV

buildup, $\approx$18 kJ/mol, turned out to be similar to that characterizing the dipolar reorientation in protiated samples.[3] This finding led us to surmise that dipolar reorientation might be the key step in the ice VI$^{\ddagger} \rightarrow$ XV transformation.[18] The problem with that conjecture is, however, that the two processes were investigated for different isotopologues. Here, we test this hypothesis by investigating the impact of isotopic substitution on both processes. Thus, we determine the ice VI$^{\ddagger} \rightarrow$ XV activation barrier for protiated samples through the rate constants determined above. We further investigate whether this isotope effect differs from that characterizing the dipole reorientation. Hence, we will present dielectric relaxation spectra on ice XIX samples featuring different H/D ratios.

Dielectric relaxation spectra of such samples provide a means to better understand the relation of two so far independently discussed effects induced by isotopic substitution. The first is the H/D isotope effect, which affects the dynamics of the ice lattice and which for samples featuring a larger D fraction typically leads to an increase of the phase transition temperature.[25–28] The second concerns the isotopic doping discussed above, which in our situation implies that ice XIX forms only for isotopic compositions of 0.5%–100% H_2O, but not for <0.04% H_2O.[1] This latter observation confirms the existence of a second isotope effect that is caused by introducing small amounts of H. The existence of two different H/D isotope effects raises the question on how these relate to each other. The evaluation of the influence of different isotopic ratios on the dynamics of the different ices should help to address that question.

II. METHODS

A. Ice XIX preparation

The samples were prepared from solutions containing <0.04, 0.5, 5, 30, and 95 wt. % of H_2O and 0.01M DCl (0.01M HCl for 95 wt. % of H_2O) in D_2O according to the previous synthesis protocol.[1,4,18] In short, the solutions were pipetted into an indium cylinder, which was placed into the bore of a steel cylinder and quenched in liquid nitrogen. This procedure led to rapid ice freezing at ambient pressure with cooling rates varying from 60 to 140 K/min. In a next step, compression was applied with a piston-cylinder setup in the universal testing machine ZWICK BZ100/TL3S to trigger pressure-induced amorphization above 1 GPa, yielding high-density amorphous (HDA) ice. HDA was then heated to 255 K, while staying at 1.8 GPa, which led to pure ice VI. In a next step, the crystal was quickly cooled at 1.8 GPa to 160 K. Up to that point, the sample remains ice VI. Then, it was slowly ramped to 90 K with rates of 0.5 K/min (3 K/min for the 95 wt. % H_2O sample). In that process, ice XIX evolved in all samples except for that with <0.04 wt. % H_2O. Ultimately, all samples were quenched to 77 K, taken out of the pressure vessel, and stored in liquid nitrogen for subsequent analysis at (sub)ambient pressure through Raman scattering in Innsbruck and dielectric spectroscopy in Dortmund.

B. Raman spectroscopy

Raman spectra in isothermal waiting experiments were recorded as described elsewhere.[3,17,18] The measurements were performed with a confocal WITec alpha300R Raman microscope, using a laser operated at a wavelength of 532 nm and a power output of 20 mW. The sample was illuminated in confocal geometry

through a ZEISS LD PlanNEOFLUAR/40× objective. The spectra were recorded through a 600 gr/mm grating with a CCD-camera. Integration times of 2–15 min had to be utilized. Due to the small cross sections in the spectral ranges containing the Raman marker bands, shorter integration times were not sufficient to achieve an acceptable signal-to-noise ratio. The sample itself was loaded into an Oxford N Microstat at 84 K, evacuated to 8 mbar, and then heated to the desired temperature. Temperature stability (±0.2 K) was achieved through a Lakeshore 331S controller, including a Pt100 heating element.

1. Analysis of ice fractions using Raman superposition

We employ the previously outlined marker bands[18] for the distinction of ices XV and XIX from ices VI and VI‡. The most prominent marker band for ice XV is in the librational range extending from 250 to 600 cm^{-1} in 5% H_2O samples and from 350 to 700 cm^{-1} in 95% H_2O samples. The marker band for ice XIX is in the decoupled stretching vibration range (3250–3500 cm^{-1} in 5% H_2O samples and 2400–2550 cm^{-1} in 95% H_2O samples). Fractions of ice XIX have been determined through superposition of the Raman spectra in these ranges and comparison with ice XIX and ice VI reference spectra in the decoupled OH/OD-stretching range. To assess the ice XV fractions, on the other hand, we utilized ice VI and ice XV reference spectra in the librational range.

For the superposition analysis of the ice XIX decay, the spectrum that was recorded first at the respective temperature ($T \geq 100$ K) is used as the ice XIX reference spectrum. Reference spectra at lower temperatures cannot be employed. For the ice XV buildup, spectra of undoped ice VI can be utilized as the ice VI‡ reference at any temperature used in this work. In the analysis, one needs to take into account that an initial ice XV fraction builds up during the prior heating process, i.e., even before the start of each isothermal waiting experiment.

An example for a superposition analysis for ice XV-buildup is presented as supplementary material in Fig. S4.

2. Modified JMAK fits to determine kinetic parameters

Following Ref. 18, the development of the ice XV and XIX fractions discussed in Sec. II B 1 can be determined as a function of time t. Then, the fractions $f(\text{XIX})$ for the ice XIX decay and $f(\text{XV})$ for the ice XV buildup were fitted using the modified JMAK model,[29]

$$f(\text{XIX}) = c^{\text{XIX}} \cdot e^{-(k(T)^{\text{XIX}}t)^{n^{\text{XIX}}}}, \quad (2a)$$

$$f(\text{XV}) = c^{\text{XV}} \cdot \left(1 - e^{-\left(k(T)^{\text{XV}}t\right)^{n^{\text{XV}}}}\right). \quad (2b)$$

In this manner, we determined the initial fraction c^{XIX} and ultimate fraction c^{XV}, the rate constants k^{XIX} and k^{XV}, and the Avrami exponents n^{XIX} and n^{XV} for each process. Equations (2a) and (2b) have proven empirically to provide more consistent rate constants than the original JMAK equation.[19]

In order to apply these fits, the initial ice XV fraction from the superposition analysis has to be set to zero even if initially there is some ice XV present. Therefore, from Eq. (2b), the freshly developed fraction of ice XV rather than the absolute fraction is calculated. The fitting curves do not necessarily converge to a $f(\text{XV})$ fraction

of 100%, i.e., to pure ice XV. In some cases—especially at elevated temperatures—residual ice VI‡ or ice VI remains, which can be rationalized if (partially) disordered domains of ice XV coexist with ordered ice XV domains. For instance, stress at junctions of ice XV domain walls might prevent H ordering in their immediate vicinity. Therefore, for $t \rightarrow \infty$, the upper limit of the ice XV buildup may vary and cannot be assumed to be 100%, but instead is described by the parameter c^{XV} ($0 < c^{XV} < 1$).

3. Arrhenius plots for activation barriers

Isothermal waiting experiments have been applied at different temperatures. Consequently, the temperature dependence of the rate constants can be investigated, allowing one to assess the activation barrier for the ice XIX decay and for the ice XV buildup. To determine the respective barriers, the rates derived from the JMAK fits are determined using the Arrhenius equation,[30]

$$k(T) = A \cdot e^{-\frac{E_A}{R \cdot T}}, \tag{3}$$

with k representing the rate constant, A representing the pre-exponential factor, and E_A representing the activation energy.

C. Dielectric relaxation spectroscopy

For the dielectric measurements, an Alpha Analyzer from Novocontrol was utilized.[31] In a first step, the samples were powdered in cold nitrogen vapor and transferred into a parallel-plate capacitor at 77 K. The temperature was regulated using a Quatro system by a stream of precooled nitrogen gas. Depending on the lowest measuring frequency, an isothermal frequency scan took about 8–45 min. During the frequency scans, the temperature was stabilized within 0.1 K. Stabilization times are 3–7 min. Detailed temperature protocols are depicted as supplementary material in Fig. S5.

Dielectric relaxation spectra were recorded for two purposes: First, the impact of the isotopic mixture on the reorientational dynamics was scrutinized in order to determine the relation of the two isotope effects that are relevant for ice XIX. Second, this method was applied in order to test the hypothesis whether or not dipole reorientation might be the rate determining step in the ice VI‡ → XV transition. Dipoles reorienting with a time constant τ lead to a peak in the dielectric loss ε'' at a frequency ν_{max} so that the relaxation time τ for the respective process can be determined through

$$\tau = \frac{2\pi}{\nu_{max}}. \tag{4}$$

The activation barrier E_R against dipole reorientation within a specific ice polymorph can be determined from the dielectric relaxation times. Analogous to Eq. (3), for dipolar reorientations, the Arrhenius equation is written as

$$\tau(T) = \tau_0 \cdot e^{\frac{E_R}{R \cdot T}}, \tag{5}$$

where τ_0 represents the pre-exponential factor. In addition to the determination of the activation barrier, the temporal evolution of the corresponding ice fractions can also be monitored and analyzed analogous to Eq. (2).
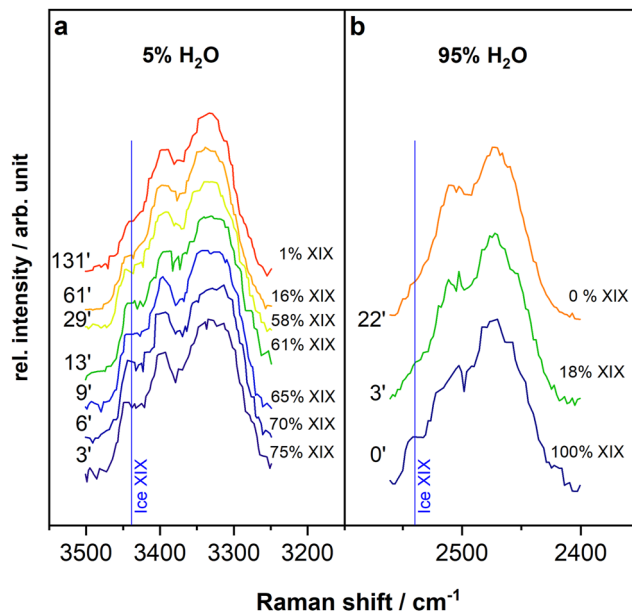

FIG. 1. Ice XIX decay at 104 K. (a) Decoupled Raman OH stretching bands in the D_2O matrix of 5% H_2O (in D_2O) ice XIX samples (adapted from Ref. 18) recorded after the given waiting time (in minutes). (b) Decoupled Raman OD stretching bands in the H_2O matrix of 95% H_2O (in D_2O) ice XIX samples. Vertical lines represent marker bands for ice XIX. The time that has passed in the isothermal experiment and the result of the superposition analysis are indicated. In this on-the-fly experiment, the high noise level is due to the short accumulation times.

III. RESULTS AND DISCUSSION

A. Influence of H/D-isotopic substitution on the ice XIX → ice VI‡ stage

We performed isothermal waiting experiments to investigate the two stages of the order–order transition, i.e., ice XIX → VI‡ and ice VI‡ → XV. Like in Ref. 18, the development of both transitions is scrutinized using Raman spectroscopy. The decay of ice XIX is discussed first: Fig. 1 shows how the ice XIX fraction develops as a function of the waiting time. The decoupled stretching vibrations of the 5% H_2O samples from Ref. 18, see Fig. 1(a), are compared with those of 95% H_2O samples; see Fig. 1(b). The fractions of residual ice XIX are analyzed through spectral superposition, cf. Sec. II B 1, and are indicated to the right of each spectrum.

It turns out that the spectrum recorded for the 5% H_2O sample at the start of the experiment, Fig. 1(a), is better resolved than the corresponding spectrum of the 95% H_2O sample, Fig. 1(b). This difference can be seen best through the ice XIX marker bands: Whereas a fully distinct peak maximum is observed for the 5% H_2O ice XIX marker band, only a shoulder can be observed for the 95% H_2O marker band. This observation implies that the ice XIX decay of 95% protiated samples might already have progressed prior to the isothermal waiting experiment.

Although the shoulder of the XIX marker band is clearly visible at the start of the isothermal waiting experiment ("0 min"), it diminishes rapidly after less than 3 min; cf. Fig. 1(b). In addition, the superposition analysis indicates that no more than 18% of the initial

TABLE I. Ice XIX decay: Rate constants k^{XIX}, Avrami exponents n^{XIX}, and KIE, see Eq. (1), as derived from the JMAK plots shown in Figs. 3(a) and 3(b).

H_2O fraction (wt. %)	T (K)	k^{XIX} (min^{-1})	n^{XIX}	KIE
5	101	9×10^{-3}	0.8	
5	104	2.5×10^{-2}	1.4	≈ 35
95	104	$\approx 9 \times 10^{-1}$	0.4	
5	108	6×10^{-2}	1.1	

ice XIX is left. The decay is complete after less than 22 min. At that point, the top spectrum in Fig. 1(b) no longer contains traces of the ice XIX marker band. It took about two minutes to record a Raman spectrum at an acceptable signal-to-noise ratio; cf. Sec. II B. Consequently, the error bars of all fit parameters describing the decay of protiated (95% H_2O) ice XIX are large.

By contrast, 95% deuterated ice XIX is still present in small amounts even after 2 h; see the top spectrum in Fig. 1(a). The slower decay of 95% deuterated ice XIX allows us to track it for temperatures up to 108 K (see Table I). At 104 K, the decay of the marker bands for the protiated samples turns out to be faster than that for the deuterated samples at 108 K. There, the ice XIX marker band of the deuterated sample is still discernible after 37 min. In summary, the ice XIX decay turns out to be significantly faster for the protiated (95% H_2O) than for the deuterated (5% H_2O) samples.

B. Influence of H/D isotopic substitution on the ice VI‡ → ice XV stage

The second stage of the ice XIX → XV transition involves the buildup of ice XV from ice VI‡. It can be examined through a superposition analysis of the Raman spectra that are recorded in the librational range. Previously, for the deuterated samples, it was found that the ice XV buildup is much slower than the ice XIX decay.[18]

Figure 2 shows four sets of Raman spectra each consisting of five selected spectra from different isothermal waiting experiments. They were measured in order to determine the formation of deuterated and protiated ice XV at 108 K and near 120 K. Additional spectra demonstrating the ice XV buildup in protiated samples during isothermal waiting are shown as Fig. S2 in the supplementary material in Fig. S1. A comparison of the time development of the isotopologues at 108 K, see Figs. 2(a) and 2(b), shows that after 90 min, approximately half of the maximum ice XV fraction has emerged in both buildups.[18] Furthermore, for both isotopologues, the increase of the ice XV fractions slows down significantly after ~150 min. Analogously, when isothermally waiting near 120 K, see Figs. 2(c) and 2(d), both isotopologues are seen to have proceeded up to half of the maximum ice XV fraction after 20–30 min. For the protiated sample, the transition is in fact finished after 100 min, and in deuterated ones, it is terminated after 160 min. That is, for both isotopes, the time scales of the ice XV ordering are relatively close to one another. The small impact of the isotopic substitution strongly contrasts with its huge effect found for the ice XIX → VI‡ transition.
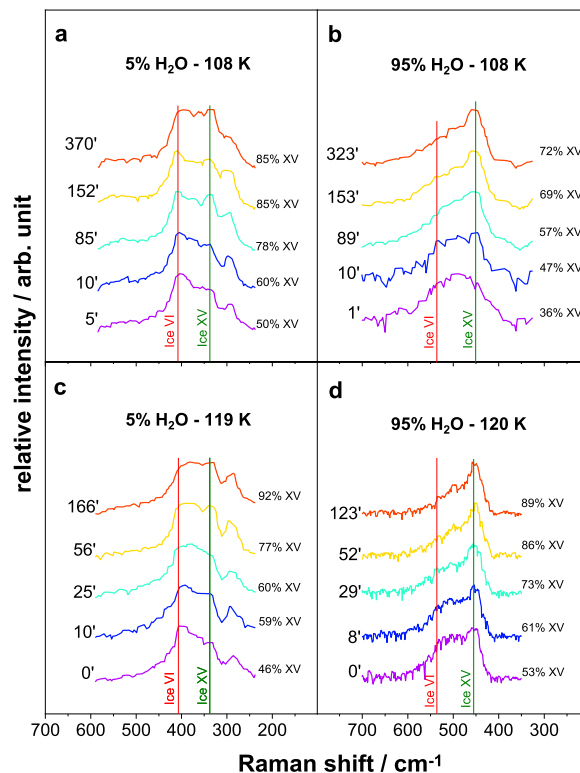

FIG. 2. Ice XV buildup at 108 K (top) and near 120 K (bottom). (a) and (c) Raman librational bands of the 5% H_2O samples (adapted from Ref. 18). (b) and (d) Raman librational bands of 95% H_2O samples. The red and green vertical lines represent marker bands for ices VI and XV, respectively. The time passed in the isothermal experiment and the ice XV fractions derived from the superposition analyses are indicated.

In addition, it is worth to compare the rate constants of the ice XIX decay and the ice XV buildup for protiated samples. It turns out that the higher rate for the ice XIX decay compared to the ice XV buildup, previously found for deuterated samples,[18] is also recognized here for the protiated samples. In fact, that difference is significantly more pronounced here.

C. Fitting with an adapted JMAK model and kinetic isotope effects for both stages

As mentioned in Sec. I, one goal of this work is to determine the KIE of the ice XIX decay and the ice XV buildup. Furthermore, the rate constants for the ice XV buildup will be utilized to reach the second goal, i.e., the determination of the activation barrier E_A for the ice VI‡ → XV transition in protiated samples. In Secs. III D and III F, the resulting barriers will be compared with those obtained for dipolar reorientation (see Ref. 3).

To this end, using the modified JMAK model, Eq. (2), we determined the rate constants for the ice XIX decay, k^{XIX}, and for the ice XV buildup, k^{XV}, from the isothermal waiting experiments depicted in Figs. 1, 2, and S1. This analysis also yielded the Avrami exponents n^{XIX} and n^{XV} as described in Sec. II B 2; see also Ref. 18.
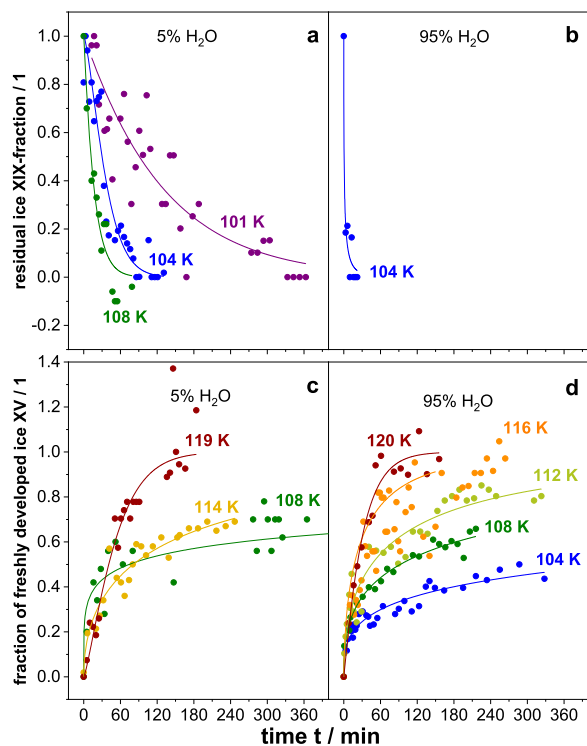
FIG. 3. Time evolution of the fractions relating to (a) and (b) the ice XIX decay and (c) and (d) the ice XV buildup as deduced from Raman superposition for different temperatures. JMAK fits are shown as solid lines. Data for the 5% H_2O samples are from Ref. 18. Avrami exponents n, rate constants k, and the resulting KIEs are summarized in Tables I and II. We estimate the error bar (one standard deviation) for the phase fractions to be ±5%.

TABLE II. Same as Table I, but for the ice XV buildup.

H_2O fraction (wt. %)	T (K)	k^{XV} (min^{-1})	n^{XV}	KIE
95	104	7×10^{-4}	0.3	
95	104	1×10^{-3}	0.4	
95	107	4×10^{-3}	0.4	
5	108	2×10^{-3}	0.2	2
95	108	3×10^{-3}	0.4	
95	108	3×10^{-3}	1.0	
95	112	1×10^{-2}	1.4	
5	114	6×10^{-3}	0.5	1
95	114	8×10^{-3}	0.4	
5	116	6×10^{-3}	0.6	3
95	116	2×10^{-2}	0.6	
5	119	2×10^{-2}	0.9	2
95	120	3×10^{-2}	1.1	
95	120	3×10^{-2}	1.1	

during the heating period preceding the isothermal waiting experiment, the ice XIX decay turns out to have progressed further for 95% H_2O than for 5% H_2O. This finding implies that in more highly protiated samples, the transition is closer to its final stage, and with argument (ii) in mind, this may explain their lower Avrami exponent.

For the ice XIX decay at 104 K, we obtain a rate constant $k_H^{XIX} \approx 0.9$ min^{-1} for the protiated samples and $k_D^{XIX} = 0.025$ min^{-1} for the deuterated samples, implying a KIE, cf. Eq. (1), of ~35. Even comparing the H_2O measurement at 104 K with the D_2O measurement at 108 K, we would still get a KIE of 15. A reason for such large KIEs could be an enhancement of the thermally activated transformation through quantum tunneling. The enhancement is particularly large if the reduced mass that moves along the reaction coordinate is low and if the temperature is low. Both conditions are met only if the H atoms jump and/or if rotations cause the ice XIX decay. In deuterated ice XIX, the reduced mass is twice as large (2 amu instead of 1 amu), and for the ice XV build-up, the temperatures are higher. In comparison to the known impact of quantum tunneling on the ice I → XI-transition,[22] the ice XIX-decay takes place at higher temperatures (104 K instead of 72 K). The reduction of the probability for quantum tunneling by thermal expansion could, however, be compensated here by the higher density in ice XIX, which is in line with the suggested impact of quantum tunneling on the ice XII → XIV-transition that takes place at a similar temperature and densities as the ice XIX decay.[24] Furthermore, the high KIE characterizing that transition is not the first hint for quantum tunneling playing a role for ice XIX. In addition, the importance of H-doping in the ice XIX-synthesis[1] can be interpreted in that direction, i.e., the effectiveness of 0.5% H_2O in D_2O in contrast to the ineffectiveness of pure D_2O despite waiting times of up to 24 h speaks in favor of quantum tunneling playing a significant role.

For the ice XV buildup, the Avrami exponent n^{XV} varies from 0.2 to 1; see Table II. Apart from a slightly higher value for the 95% H_2O sample at 112 K, a significant difference or trend between the measurements cannot be seen. An explanation for the small

Based on the data from Fig. 1, the time dependent decay of the ice XIX fraction is plotted in Figs. 3(a) and 3(b). Figures 3(c) and 3(d) summarize the buildup of ice XV for deuterated (from Ref. 18) and protiated samples (from Figs. 2 and S1). The coefficients k^{XIX}, k^{XV}, n^{XIX}, and n^{XV} as derived from the modified JMAK fits are shown in Table I for the ice XIX decay and in Table II for the ice XV buildup. By comparing the rate constants of each isotopologue, the kinetic isotope effect (KIE) has been determined through Eq. (1).

Note that only ice XV that freshly developed since the start of the experiment ("0 min") is considered in the JMAK fits and that pure ice XV does not necessarily develop in the limit of infinite waiting time.

With these provisos in mind, the fit results presented in Fig. 3 and Tables I and II can be discussed. For the protiated ice XIX decay, an Avrami exponent $n^{XIX} \approx 0.4$ is obtained. This exponent is significantly smaller than that for deuterated ice XIX, which ranges from 0.8 to 1.[18] Small Avrami exponents are (i) often caused by a limited growth of the product phase in certain directions, e.g., if large domains of the product phase prevent its further expansion. Small exponents can also arise (ii) if the nucleation rate decreases in time as is often connected with shrinking educt-phase domains during the final stage of the transition. Then, the decreasing educt phase provides fewer nucleation sites.[32,33] As shown in Sec. III A,

exponents could be an impeded growth between two differently oriented ice XV domains, possibly connected with differences of the initial orientations of the ice XV nuclei that hampers consistent H ordering. These effects can lead to different limiting ice XV fractions in the product phase depending on the relative orientations of the ice XV domains. This scenario is compatible with earlier calorimetric findings:[4] Thermograms recorded after recooling doped ice VI from 140 K show larger endothermic enthalpies than after recooling former ice XIX from 118 K. We attributed this difference to ice XV nucleation from ice VI‡ taking place at many different sites,[4] which, consequently, leads to the formation of differently oriented ice XV domains. Therefore, after recooling from 118 K, an increased extent of residual H disorder remains between these domains.[4] Upon recooling from 140 K, on the other hand, the growth of H order seems to dominate over nucleation effects that are prevalent at the (higher) temperatures at which the ice VI → XV transition takes place. This situation then leads to larger domain sizes and, thereby, a higher degree of H order. Based on the scatter of the Avrami exponents and the lack of a clear trend with temperature, it is difficult to deduce details regarding the physics of nucleation/growth, though.

At a given temperature, the rate constants k_D^{XV} and k_H^{XV}, see Table II, are significantly closer to each other than k_D^{XIX} and k_H^{XIX}; see Table I. Therefore, in the 108–119 K range, the KIE for the ice XV buildup is only 1–3, indeed a very small effect. This compares with a scatter of rate constants of a factor of about 2 upon reproducing an experiment.

D. Arrhenius plots for the ice XIX → VI‡ and the VI‡ → XV stages

To determine E_A for both isotopologues, in Fig. 4 we plot the rate constants k^{XIX} and k^{XV} in an Arrhenius diagram. The large difference between the rates for the ice XIX decay in 5% H_2O samples (red squares) and the rates for ice XIX decay in 95% H_2O samples (blue square) illustrates the high KIE for the ice XIX decay, see also Table I, and the much smaller one for the ice XV buildup, see Table II. From Fig. 4, it can be seen that the activation barrier E_A for the ice XV buildup in both H_2O and D_2O is about 18 kJ/mol. A comparison with the rate constant derived from dielectric spectroscopy, cf. Fig. S2, agrees with the corresponding set of Raman measurements; see the blue diamond in Fig. 4.

In fully deuterated samples, ice XIX does not form. Instead, such samples remain disordered, ice VI-like, which we refer to as ice VI*. Starting from ice VI*, instead of the ice XIX → VI‡ → XV sequence dealt with so far, a single-step ice VI* → XV transition takes place. Using dielectric spectroscopy, this transition was monitored for a <0.4% H_2O sample, see Fig. S3, and the result is represented by the brown diamond in Fig. 4. For the deuterated samples, the proximity of the VI* data point to those for the ice XV buildup (here referring to the ice VI‡ → XV transition) implies that both transformations are of a similar nature. That is, the crystallographic distortion[14] that potentially distinguishes ice VI* from ice VI‡ does not affect the kinetics of the ice XV buildup significantly.

E. Dielectric spectroscopy: Impact of isotopic composition on the reorientational dynamics

By studying samples with different H/D fractions, dielectric measurements were performed with the goal to elucidate the relation
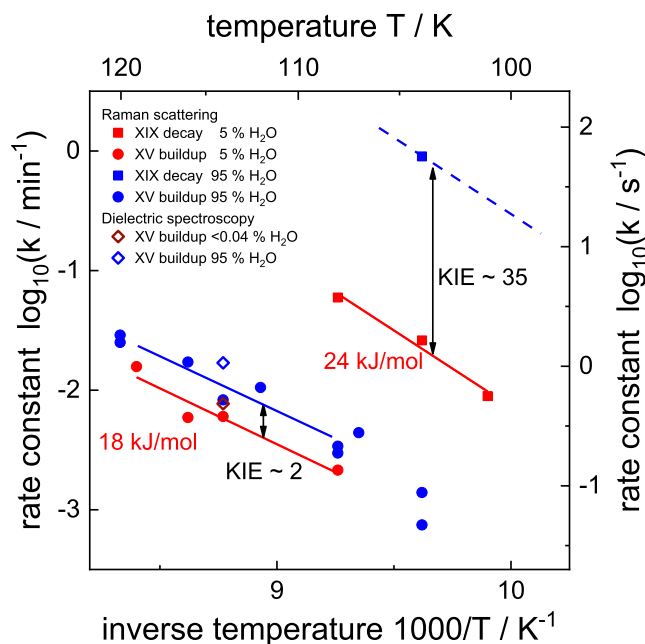

FIG. 4. Arrhenius plot for the ice XIX decay (squares) and the ice XV buildup (circles and diamonds) recorded for different isotopic mixtures (blue for 95% H_2O, red for 5% H_2O, and brown for <0.04% H_2O) and methods (filled squares and circles for Raman spectroscopy and diamonds for dielectric spectroscopy derived from Figs. S2 and S3). The solid lines represent Arrhenius laws with the given energy barriers; the dashed line is drawn to guide the eye.

between the H/D isotope effect in the crystal lattice and the effect of H doping. To illustrate the impact of the isotopic composition on the dielectric relaxation spectra, Fig. 5 shows dielectric loss spectra of samples with H_2O contents of 95%, 30%, 0.5%, and <0.04%. The timescale of the heating process is depicted for each sample in Fig. S5. Starting from a temperature of 97 K, loss spectra were recorded upon heating. Above 100 K, for all samples, except for that containing <0.04% H_2O, well-defined dielectric loss peaks are observed. The low-frequency side of the spectra is broadened in all cases, which was similarly reported also for other crystalline ices.[11,34] Furthermore, it is seen that toward low frequencies, most peaks are overlaid by an ε'' increase. Arising from the presence of a residual electrical conductivity, this feature is also well known from other ice crystals, particularly from those featuring ionic doping.[11,34] For the sample containing <0.04% H_2O, peaked dielectric losses are only observed below about 119 K. For higher temperatures, peaks are not discernible so that the characteristic time scales had to be estimated using a procedure called frequency–temperature superposition.[35] Basically, this means that in the high-temperature regime, the spectra were shifted (here: using semi logarithmic plots) along the frequency axis to achieve an approximate overlap of their well-defined high-frequency flanks. From the shift factors, the effective time scales characterizing the corresponding spectra could be assessed. For low temperatures and for all other samples, τ was directly determined by means of Eq. (4).

Comparing the peak positions at the highest temperatures for different measurements, one observes that for the 95% H_2O sample,
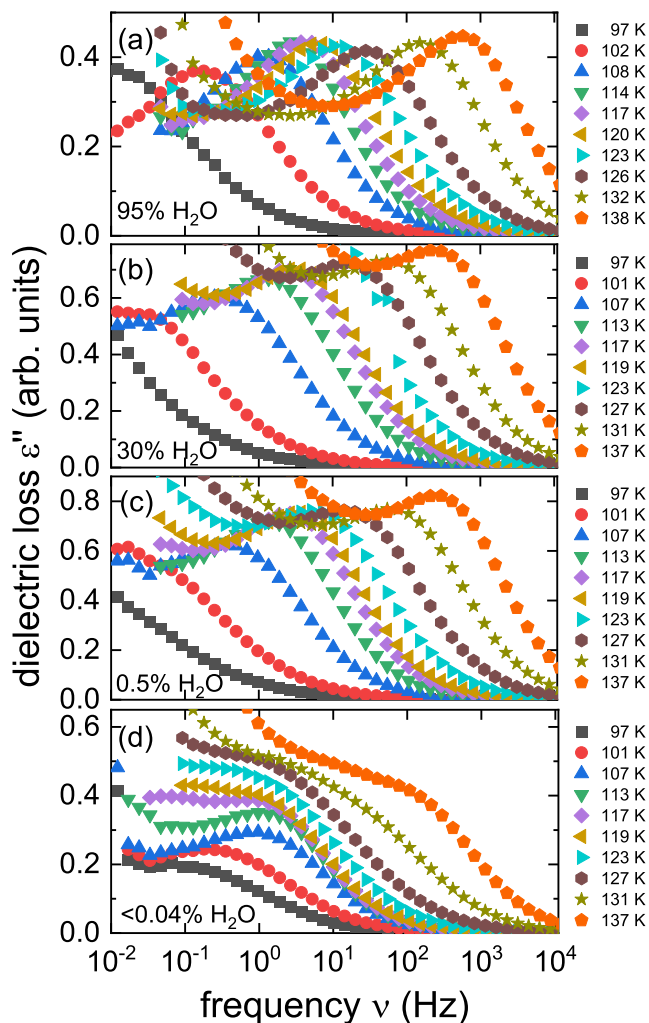
FIG. 5. Dielectric relaxation spectra of ice crystals with H_2O fractions of (a) 95%, (b) 30%, (c) 0.5%, and (d) <0.04%.
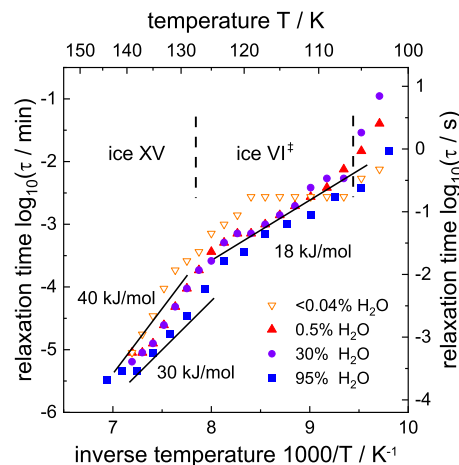

FIG. 6. Arrhenius diagram showing the relaxation times recorded upon heating for ices with different isotopic compositions. The data for the <0.04% H_2O sample are shown as open symbols to indicate that due to the application of frequency–temperature superposition, the accuracy of the time scales obtained for this concentration may be somewhat reduced. The given energy barriers are represented by the solid lines. The dashed lines mark the temperature range in which ice VI‡ exists.

see Fig. 5(a), the loss peak maximum occurs at the highest frequency. Even taking into account that for the 95% sample a slightly larger temperature was measured, it displays the fastest dipole reorientation. Between 108 and 126 K, the spectra shift less than they do at higher and at lower temperatures. Above 126 K, the transition to ice VI occurs, such as for all samples studied here.

The samples containing H_2O fractions of 30% and 0.5% H_2O, see Figs. 5(b) and 5(c), respectively, resemble the pattern observed for 95% H_2O. However, a close inspection of the spectra, see, for instance, at 107 K, reveals that for 30% and 0.5% H_2O, the peak frequencies are close to each other and smaller than for the more fully protiated sample. This finding is compatible with the expectation that the presence of a larger fraction of heavier isotopes should lead to slower dynamics. Analogous effects are known, e.g., for deuterated ice XII and ice XIV. These crystals show peak frequencies, which are 10–30 smaller than for their protiated counterparts.[34] In addition, the dynamics of the deuterated ices I and

XI is about ten times slower as compared to the corresponding protiated ices.[36]

At high temperatures, the <0.04% H_2O sample shows effective time scales that are the longest among the studied samples, in line with their maximum degree of deuteration. The *low*-temperature spectra shown in Fig. 5(d) reveal, however, *higher* peak frequencies than for most partially protiated samples. At first sight, this latter finding seems counterintuitive. It can, however, be understood when taking into account that samples with <0.04% H_2O do not form ice XIX,[1] but remain in the H-disordered ice VI* state at low temperatures. Dielectric relaxation spectra of such samples are, in general, shifted to higher frequencies compared to their H-ordered counterparts. Below the ice I → XI, ice V → XIII, and ice XII → XIV transitions, the reorientational energy barriers are larger than in the H-disordered phase.[11,12,36] In other words, at low temperatures, the peak frequencies remain higher in the H-disordered than in the ordered state. This situation also obviously applies when comparing the dynamics of the <0.04% ice VI* sample with that of the ice XIX samples.

Another observation, which refers to the <0.04% H_2O sample, is that its spectra show little thermal evolution for temperatures between about 107 and 120 K. In this range, see Secs. III B–III D, for samples originating from ice XIX, the ice VI‡ → XV transition is taking place. We speculate that for the <0.04% H_2O sample, analogously, the ice VI* → XV transition occurs in the same interval. To rationalize the almost temperature invariant peak frequencies, we may thus invoke two counteracting effects: While an increasing thermal activation speeds up the dynamics upon heating, the successive H-ordering accompanying the ice VI* → XV transition slows it down. Thus, in an intermediate temperature range, the two tendencies more or less compensate, thus leading to an almost vanishing effective energy barrier. For the other samples, the compensation

of the thermal activation and H-ordering effects is not quite as balanced, but nevertheless gives rise to a reduced energy barrier as will be shown in the following.

To obtain the activation barriers E_R against dipolar reorientation in the various temperature ranges, using Eq. (5), we analyzed the data shown in Fig. 5 and summarize the results in an Arrhenius plot; see Fig. 6. In the high-temperature regime, in which ice XV transforms to ice VI, E_R is in the range of 30–40 kJ/mol, in harmony with values found for the same temperature interval on protiated samples, which yielded 30–34 kJ/mol.[3] As shown in Secs. III A–III D, at temperatures above 108 K up to at least 120 K, ice VI‡ and ice XV are prevalent. In that range, the samples with $\geq 0.5\%$ H_2O are characterized by a barrier of about 18 kJ/mol, again in agreement with the results from Ref. 3 where the same value was reported.

As shown in Sec. III D, the activation barrier E_A characterizing the kinetics of the ice VI‡ → XV transition in deuterated samples is again ~18 kJ/mol. It is remarkable that the isotopic substitution does not significantly alter any of these barriers. The agreement of E_A and E_R suggests that dipole reorientation might indeed be the rate determining step in the ice VI‡ → XV transition.

IV. CONCLUSIONS

In the present work, we investigated kinetic isotope effects of each stage in the ice XIX → VI‡ → XV transition sequence, thereby shedding light on the mechanism underlying the only order-to-order transition known in ice physics. For that purpose, we measured a series of Raman spectra during isothermal waiting experiments on H_2O ice XIX samples. Using this data base, we retrieved the kinetics of the ice XIX → VI‡ → XV transition sequence, analogous to that of the previously studied deuterated samples.[18] Comparing the results of the protiated with those of the deuterated samples, we determined the KIE for each transition step.

It turns out that the ice XIX decay displays a significant isotope effect. This is, for instance, seen from Fig. 1, where at 104 K the marker band for D_2O ice XIX can still be observed after 131 min, while that of H_2O ice XIX vanishes already after 22 min. Consequently, for the ice XIX → VI‡ transition, the Arrhenius diagram (Fig. 4) shows a huge gap between the rate constants of H_2O and that of D_2O samples. This finding supports the hypothesis that quantum tunneling might contribute to the rate for the transition from protiated ice XIX to ice VI‡.

Conversely, the ice XV buildup is not only much slower than the ice XIX decay, but it also shows a much smaller KIE. The pronounced difference in the KIEs for the buildup and the decay stages implies mechanistic differences regarding the two transformations. In other words, H-transfer possibly enhanced by tunneling effects seems to play a larger role in the ice XIX-decay compared to the ice XV-buildup.

Furthermore, the relation between the influence of the H/D substitution on the lattice and the necessity of H doping as a prerequisite for ice XIX formation is investigated. For that purpose, we measured dielectric loss spectra for samples with different isotopic compositions. Samples with H_2O fractions of 0.5% and 30% show essentially the same dynamics. Reducing the H_2O fraction to <0.04%

leads to a significant slowdown of the dynamics, and increasing it to 95% H_2O yields an enhancement.

Moreover, for all samples, the activation barriers E_R against dipole reorientation were determined from the dielectric loss spectra. These barriers turn out to be similar to the activation barriers E_A that relate to the ice VI‡ → XV transition. This similarity vindicates the suggestion that dipole reorientation is the rate determining step for the ice XV buildup.

SUPPLEMENTARY MATERIAL

The supplementary material includes additional Raman data for ice XV build-up (Fig. S1) and a comparison of Avrami plots based on dielectric and Raman data (Figs. S2 and S3), including kinetic parameters (Table S1). Furthermore, it shows an example for the Raman superposition analysis to determine fractions of ices (Fig. S4) and heating protocols for dielectric measurements (Fig. S5).

ACKNOWLEDGMENTS

AUTHOR DECLARATIONS
Conflict of Interest

The authors have no conflicts to disclose.

Author Contributions

Alexander V. Thoeny: Conceptualization (supporting); Data curation (lead); Formal analysis (lead); Investigation (lead); Methodology (lead); Visualization (lead); Writing – original draft (lead); Writing – review & editing (lead). **Tobias M. Gasser**: Data curation (supporting); Formal analysis (supporting); Investigation (equal); Writing – review & editing (supporting). **Lars Hoffmann**: Data curation (equal); Formal analysis (equal); Investigation (equal); Methodology (equal); Writing – review & editing (supporting). **Markus Keppler**: Data curation (supporting). **Roland Böhmer**: Conceptualization (equal); Formal analysis (equal); Methodology (equal); Supervision (equal); Writing – review & editing (equal). **Thomas Loerting**: Conceptualization (lead); Formal analysis (supporting); Project administration (lead); Writing – original draft (supporting); Writing – review & editing (equal).

DATA AVAILABILITY

The data that support the findings of this study are available from the corresponding author upon reasonable request.

REFERENCES

[1] T. M. Gasser, A. V. Thoeny, A. D. Fortes, and T. Loerting, "Structural characterization of ice XIX as the second polymorph related to ice VI," Nat. Commun. **12**, 1128 (2021).

[2] R. Yamane, K. Komatsu, J. Gouchi, Y. Uwatoko, S. Machida, T. Hattori, H. Ito, and H. Kagi, "Experimental evidence for the existence of a second partially-ordered phase of ice VI," Nat. Commun. **12**(1), 1129 (2021).

[3] T. M. Gasser, A. V. Thoeny, L. J. Plaga, K. W. Köster, M. Etter, R. Böhmer, and T. Loerting, "Experiments indicating a second hydrogen ordered phase of ice VI," Chem. Sci. **9**(18), 4224–4234 (2018).

[4] T. M. Gasser, A. V. Thoeny, V. Greussing, and T. Loerting, "Calorimetric investigation of hydrogen-atom sublattice transitions in the ice VI/XV/XIX trio," J. Phys. Chem. B **125**(42), 11777–11783 (2021).

[5] C. G. Salzmann, P. G. Radaelli, E. Mayer, and J. L. Finney, "Ice XV: A new thermodynamically stable phase of ice," Phys. Rev. Lett. **103**(10), 105701 (2009).

[6] S. Kawada, "Dielectric dispersion and phase transition of KOH doped ice," J. Phys. Soc. Jpn. **32**(5), 1442 (1972).

[7] S. J. Laplaca, W. C. Hamilton, B. Kamb, and A. Prakash, "On a nearly proton-ordered structure for ice IX," J. Chem. Phys. **58**(2), 567–580 (1973).

[8] G. P. Johari, A. Lavergne, and E. Whalley, "Dielectric properties of ice VII and VIII and the phase boundary between ice VI and VII," J. Chem. Phys. **61**(10), 4292–4300 (1974).

[9] C. G. Salzmann, P. G. Radaelli, A. Hallbrucker, E. Mayer, and J. L. Finney, "The preparation and structures of hydrogen ordered phases of ice," Science **311**(5768), 1758–1761 (2006).

[10] A. Polian and M. Grimsditch, "New high-pressure phase of H$_2$O: Ice-X," Phys. Rev. Lett. **52**(15), 1312–1314 (1984).

[11] K. W. Köster, A. Raidt, V. Fuentes Landete, C. Gainaru, T. Loerting, and R. Böhmer, "Doping-enhanced dipolar dynamics in ice V as a precursor of hydrogen ordering in ice XIII," Phys. Rev. B **94**(18), 184306 (2016).

[12] K. W. Köster, V. Fuentes-Landete, A. Raidt, M. Seidl, C. Gainaru, T. Loerting, and R. Böhmer, "Dynamics enhanced by HCl doping triggers 60% Pauling entropy release at the ice XII–XIV transition," Nat. Commun. **6**(1), 7349 (2015).

[13] J. J. Shephard and C. G. Salzmann, "The complex kinetics of the ice VI to ice XV hydrogen ordering phase transition," Chem. Phys. Lett. **637**, 63–66 (2015).

[14] C. G. Salzmann, J. S. Loveday, A. Rosu-Finsen, and C. L. Bull, "Structure and nature of ice XIX," Nat. Commun. **12**(1), 3162 (2021).

[15] K. Komatsu, "Neutrons meet ice polymorphs," Crystallogr. Rev. **28**(4), 224–297 (2022).

[16] B. Kamb, "Structure of ice VI," Science **150**, 205 (1965).

[17] A. V. Thoeny, T. M. Gasser, and T. Loerting, "Distinguishing ice β-XV from deep glassy ice VI: Raman spectroscopy," Phys. Chem. Chem. Phys. **21**(28), 15452–15462 (2019).

[18] A. V. Thoeny, I. S. Parrichini, T. M. Gasser, and T. Loerting, "Raman spectroscopy study of the slow order-order transformation of deuterium atoms: Ice XIX decay and ice XV formation," J. Chem. Phys. **156**(15), 154507 (2022).

[19] Y. Khanna and T. Taylor, "Comments and recommendations on the use of the Avrami-equation for physicochemical kinetics," Polym. Eng. Sci. **28**, 1042–1045 (1988).

[20] R. A. M. O'Ferrall, "A pictorial representation of zero-point energy and tunnelling contributions to primary hydrogen isotope effects," J. Phys. Org. Chem. **23**(7), 572–579 (2010).

[21] W. H. Saunders, "Kinetic isotope effects," in *Survey of Progress in Chemistry*, edited by A. F. Scott (Elsevier, 1966), pp. 109–146, ISBN: 0081-976X.

[22] A. H. Castro Neto, P. Pujol, and E. Fradkin, "Ice: A strongly correlated proton system," Phys. Rev. B **74**(2), 024302 (2006).

[23] M. Benoit, D. Marx, and M. Parrinello, "Tunnelling and zero-point motion in high-pressure ice," Nature **392**(6673), 258–261 (1998).

[24] C. M. Tonauer, E. Hauschild, S. Eisendle, V. Fuentes-Landete, K. Yamashita, L. Hoffmann, R. Böhmer, and T. Loerting, "Strategies to obtain highly ordered deuterated ices presented on the example of ice XIV," PNAS Nexus **2**(12), pgad418 (2023).

[25] V. K. L. Mer and W. N. Baker, "The freezing point of mixtures of H$_2$O and D$_2$O. The latent heat of fusion of D$_2$O," J. Am. Chem. Soc. **56**(12), 2641–2643 (1934).

[26] V. Fuentes-Landete, S. Rasti, R. Schlögl, J. Meyer, and T. Loerting, "Calorimetric signature of deuterated ice II: Turning an endotherm into an exotherm," J. Phys. Chem. Lett. **11**(19), 8268–8274 (2020).

[27] S. Lemke, P. H. Handle, L. J. Plaga, J. N. Stern, M. Seidl, V. Fuentes-Landete, K. Amann-Winkel, K. W. Köster, C. Gainaru, T. Loerting, and R. Böhmer, "Relaxation dynamics and transformation kinetics of deeply supercooled water: Temperature, pressure, doping, and proton/deuteron isotope effects," J. Chem. Phys. **147**(3), 034506 (2017).

[28] T. Matsuo, Y. Tajima, and H. Suga, "Calorimetric study of a phase transition in D$_2$O ice doped with KOD: Ice XI," J. Phys. Chem. Solids **47**(2), 165–173 (1986).

[29] D. W. Henderson, "Thermal analysis of non-isothermal crystallization kinetics in glass forming liquids," J. Non-Cryst. Solids **30**(3), 301–315 (1979).

[30] S. Arrhenius, "Über die Reaktionsgeschwindigkeit bei der Inversion von Rohrzucker durch Säuren," Z. Phys. Chem. **4U**(1), 226–248 (1889).

[31] L. J. Plaga, A. Raidt, V. Fuentes Landete, K. Amann-Winkel, B. Massani, T. M. Gasser, C. Gainaru, T. Loerting, and R. Böhmer, "Amorphous and crystalline ices studied by dielectric spectroscopy," J. Chem. Phys. **150**(24), 244501 (2019).

[32] P. Bruna, D. Crespo, R. González-Cinca, and E. Pineda, "On the validity of Avrami formalism in primary crystallization," J. Appl. Phys. **100**(5), 054907 (2006).

[33] G. Zahn, P. Zerner, J. Lippke, F. L. Kempf, S. Lilienthal, C. A. Schröder, A. M. Schneider, and P. Behrens, "Insight into the mechanism of modulated syntheses: *In situ* synchrotron diffraction studies on the formation of Zr-fumarate MOF," CrystEngComm **16**(39), 9198–9207 (2014).

[34] V. Fuentes-Landete, K. W. Köster, R. Böhmer, and T. Loerting, "Thermodynamic and kinetic isotope effects on the order–disorder transition of ice XIV to ice XII," Phys. Chem. Chem. Phys. **20**(33), 21607–21616 (2018).

[35] J. Stern, M. Seidl, C. Gainaru, V. Fuentes-Landete, K. Amann-Winkel, P. H. Handle, K. W. Köster, H. Nelson, R. Böhmer, and T. Loerting, "Experimental evidence for two distinct deeply supercooled liquid states of water—Response to 'Comment on 'Water's second glass transition,' by G.P. Johari, Thermochim. Acta (2015)," Thermochim. Acta **617**, 200–207 (2015).

[36] S. Kawada, "Dielectric properties of KOH-doped D$_2$O ice," J. Phys. Soc. Jpn. **58**(1), 295–300 (1989).